J Nanopart Res (2011) 13:4947–4956
DOI 10.1007/s11051-011-0474-0

RESEARCH PAPER

Electronic properties of a zinc oxide nanotube under uniaxial tensile strain: a density functional theory study

Shin-Pon Ju · Meng-Hsiung Weng · Chia-Hung Lee

Received: 4 May 2011 / Accepted: 21 June 2011 / Published online: 15 July 2011

Abstract In this article, density functional theory calculations were employed to investigate the electronic properties of (4,4) armchair zinc oxide single-walled nanotubes (ZNONTs) under uniaxial mechanical deformations. It was found that the highest-occupied molecular orbital and the lowest-unoccupied molecular orbital gap and the value of radial buckling will both decrease linearly with the increase of axial strain. The elongation of the ZNONT mainly originates from the decrease and increase of two characteristic bond angles rather than Zn–O ionic bond elongation. This mechanical behavior is very different from the uniaxial tensional processes of carbon nanotubes and silicon carbide nanotubes formed by covalent bonds. The partial densities of states of the Zn atom and O atom show that the unoccupied states are gradually left-shifted as ZNONT elongates from 0 to 15%. Neither Mulliken charge nor deformation density clearly changes with the different tension strains. Bond order analysis also indicates the bonding strength will decrease as the strain increases from 0 to 15%.

S.-P. Ju (✉) · M.-H. Weng · C.-H. Lee
Department of Mechanical and Electro-Mechanical Engineering, Center for Nanoscience and Nanotechnology, National SunYat-Sen University, Kaohsiung 804, Taiwan, ROC
e-mail: jushin-pon@mail.nsysu.edu.tw

Keywords Zincoxide nanotubes · DFT · Mechanical properties · Electronic properties · HOMO · LUMO · Modeling and simulation

Introduction

In recent decades, the II–VI compounds have attracted considerable interest because they have broad applications in different areas, such as in photovoltaic solar cells (Ferekides and Britt 1994; Chou et al. 1996; Niemegeers and Burgelman 1997; Touskova et al. 1997; Keis et al. 2002), optical sensitizers (Sebastian and Ocampo 1996), and quantum devices. Bulk zinc oxide (ZnO), one of the II–VI semiconductor material compounds, possesses unique physical properties (e.g., a wide direct band gap of 3.37 eV and a large excitation binding energy of 60 MeV) and is very suitable for applications in electronic and optical devices (Chubachi 1976). Except for ZnO polycrystalline, ZnO materials have also been demonstrated to be highly sensitive gas sensors. Since ZnO polycrystalline with grain boundaries has limited surfaces for gas adsorption, its sensitivity as a gas sensor is decreased (Sberveglieri et al. 1995; Rao 2000; Xu et al. 2000; Chu et al. 2005; Ozgur et al. 2005; Tien et al. 2005; Liao et al. 2007).

Among these ZnO materials, ZnO nanorods were first reported in 2001 (Huang et al. 2001). Since then, various kinds of ZnO one-dimensional nanostructures have been widely investigated by experiment

(Sberveglieri et al. 1995; Rao 2000; Xu et al. 2000; Chu et al. 2005; Ozgur et al. 2005; Tien et al. 2005; Liao et al. 2007; Fulati et al. 2009; Kong et al. 2003, 2009; Liu et al. 2009; Wang et al. 2003; Kluth et al. 1999; Das and Ray 2003; Rodriguez et al. 2000; Jing et al. 2004). Single-walled zinc oxide nanotubes (ZNONTs) have attracted especially great interest because they have higher surface-to-volume ratios for potential use in different technologies, such as gas sensors (Sberveglieri et al. 1995; Rao 2000; Xu et al. 2000; Chu et al. 2005; Ozgur et al. 2005; Tien et al. 2005; Liao et al. 2007), transparent conductive oxides (Kluth et al. 1999; Das and Ray 2003), and photo catalysts (Rodriguez et al. 2000; Jing et al. 2004). Recently, ZNONTs have been synthesized successfully by physical evaporation of a mixture of ZnO and graphite powders (Kong et al. 2003).Wang et al. (2003) also employed the vapor-phase growth to fabricate multi-wall ZNONTs on large substrates. Furthermore, Liu et al. (2009) fabricated ZNONTs on an indium tin oxide (ITO) substrate and found that the vertically aligned ZNONT arrays have a large persistence photoconductivity (PPC) such that ZNONTs can also be used as an amperometric glucose biosensor (Kong et al. 2009) and as miniaturized PH sensors (Fulati et al. 2009).

The material characteristics of ZNONTs have been widely reported by theoretical approaches (Kong et al. 2003; Erkoc and Kokten 2005; Wang et al. 2007; Xu et al. 2007; An et al. 2008; Mao et al. 2008; Yuan et al. 2008; Zhou et al. 2008; Zhu et al. 2008). Erkoc and Kokten H (2005) investigated the structural and electronic characteristic of single-walled ZNONTs in armchair (4,4) and zigzag (4,0) models by performing AM1 type semiempirical molecular and orbital calculations. Their results show that the highest-occupied molecular orbital and lowest-unoccupied molecular orbital (HOMO–LUMO) gap of these ZNONTs depended on the chirality of the tube. However, their result is different from Wang et al.'s (2007) density functional theory (DFT) study, which shows that the direct band gaps are insensitive to the structures. Wang et al. (2007) analyzed the stability and electronic structures of single-walled ZNONTs. Their conclusion is that single-walled ZNONTs have smaller strain energies compared with boron nitride (BN) nanotubes with the same diameter. Furthermore, they also found the single-walled ZNONTs are relatively stable with respect to the ZNO graphite single layer. Yuan et al. (2008) employed an atomic calculation to explore the structural and elastic properties of single-walled ZNONTs with different chiralities and radii. They found that the bond length, bond angle, and Young's modulus of ZNONTs are dependent on the chirality when the tube radius is smaller than 6 Å. In contrast, all these properties are independent of chirality when the tube radius is larger than 6 Å. Zhu et al. (2008) studied the electronic properties of (10,0) and (10,10) ZNONTs by the DFT method. Their results show the ZNONT structures are relatively stable compared with bulk ZnO material. Furthermore, their band gap is found to be larger than that of the bulk ZnO. The structural and electronic properties of different one-dimension ZnO nanostructures (faceted nanotube, conventional single-walled nanotube and nanowires) are also investigated by Zhou et al. (2008). They found that the binding energy of two ZNONTs is both higher than the ultrathin ZnO nanowires.

In addition, both experimental (Qin et al. 2008; Gao and Wang 2005; Wang et al. 2006; Wang and Song 2006; He et al. 2007) and theoretical (Kong et al. 2003; Erkoc and Kokten 2005; Wang et al. 2007; Xu et al. 2007; An et al. 2008; Mao et al. 2008; Yuan et al. 2008; Zhou et al. 2008; Zhu et al. 2008) studies have demonstrated that electronic and chemical properties of one-dimensional nanomaterials are influenced by mechanical deformation. Experimentally, Wang et al. have demonstrated the ZnO nanowire can convert different nanoscale energies (Wang and Song 2006; Qin et al. 2008), i.e., mechanical, vibrational, or hydraulic energy, into electrical energy under bending deformation. This performance indicated the ZnO nanowire has both semiconducting and piezoelectric properties. This result can provide the ZnO nanowire with some applications in energy output by material deformation. In a recent experimental application (Kaniber et al. 2009), the photocurrent properties of freely suspended single-walled carbon nanotubes were found to display a relationship to uniaxial strain. The carbon nanotubes (CNTs) were stretched uniaxially by two L-shaped fittings bonded to both sides of a piezoelectric stack, such that the CNT length could be extended if a voltage were applied to the piezoelectric stack. Theoretically, Shiri et al. (2008) studied the electromechanical properties of hydrogen passivated silicon nanowires with uniaxial tensile

strain by the tight binding method. They found the band gap of silicon nanowires depends strongly on the uniaxial strain. Furthermore, the electronic properties of a boron nitride nanotube and a silicon carbide nanotube under uniaxial tensile strain have also been explored in our previous studies (Ju et al. 2011; Chen et al. 2010). The result shows that the electronic properties are significantly affected by uniaxial strain. For example, for silicon carbide nanotube, the band gap decreasing linearly with the increase of axial strain and the partial density of state (PDOS) demonstrated that the occupied states of the Si atom and the unoccupied states of the C atom are red-shifted and blue-shifted under uniaxial tension.

Since the mechanical deformation of one-dimensional nanomaterials has considerable effect on their electronic properties, the deformed ZnO nanotube could also display different electronic properties. However, to the best of our knowledge, previous studies or detailed discussions on the effect of axial deformation on ZNONT electronic properties are still lacking. Accordingly, the purpose of the current study is to investigate the electronic properties of an armchair (4,4) single-walled ZNONT under different axial strains by DFT calculation.

Simulation model

The DFT methods, implemented in the DMol^3 package (Delley 1990, 2000), were used to study the relationship between the uniaxial strain and electronic properties of an armchair (4,4) single-walled ZNONT. This method has been widely used in the theoretical calculation of nanotube systems, including structural and electronic properties. Effective core potentials (ECPs) calculations with double numerical basis sets plus polarization functional (DNP), and the generalized approximation (GGA) (Langreth and Perdew 1980) with the Perdew–Burke–Ernzerhof (PBE) (Perdew et al. 1996) correction were employed to optimize the geometry of the ZNONT. Mulliken population analysis was employed to obtain the charge on each atom. Spin-polarization was considered in our calculation. The self-consistent field (SCF) tolerance and integration accuracy were all set to "fine" with high accuracy of 10^{-6} au for energy convergence.

A (4,4) single-walled ZNONT consisting of 48 zinc and 48 oxygen atoms was chosen as the studied system. Both ends of the ZNONT having dangling bonds terminate in hydrogen atoms. Before elongation, the ZNONT was optimized to eliminate any internal stresses. After the tube was fully relaxed, the length and diameter of the ZNONT were 18.5 and 7.35 Å, respectively. The optimized structure is shown in Fig. 1. In the axial tensile process, the Zn atoms and O atoms consist of two atomic layers at both ends of the ZNONT which are kept fixed, whereas the remaining layers are fully relaxed during the calculations. In Table 1, the material properties of several ZNONTs including the tube diameter, bond-length, binding energy, and charge transfer are shown for comparison to available previous results (Wang et al. 2007). The nanotube is more stable as the size increases because of the rise in binding energy. These results are in agreement with Wang's study (Wang et al. 2007). Furthermore, the geometries of ZNONTs from (3,3) to (5,5) are very close to those in previous studies, so the parameters used in DMol^3 can obtain reliable results.

The stress on the m plane of the nanotube in the n-direction is calculated by (Chandra et al. 2004).

$$\sigma_{mn} = \frac{1}{N_s}\sum_i \left[\frac{m v_i^m v_i^n}{v_i} - \frac{1}{2v_i}\vec{r}_i \cdot \vec{F}_i^{\text{Int}}\right] \quad (1)$$

where m is the mass of atom i, v_i^m and v_i^m are the velocity components of atom i in the m- and n-directions, respectively; v_i is the volume assigned around atom i, N_s is the number of particles contained within region S, where S is defined as the region of atomic interaction; r is the position of atom i; and F_i^{Int} is the internal force acting on atom i.

The first term on the right-hand side of Eq. 1 describes the kinetic effect of the atomic motion and is dependent on the temperature. This term is not

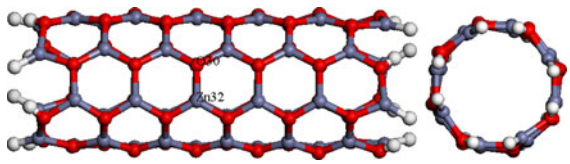

Fig. 1 Top and side views of a single wall (4,4) ZNONT. *Red* atoms are oxygen, *gray* atoms are zinc, and *white* atoms are hydrogen. [Color figure can be viewed in the online issue]

Table 1 Tube diameter, bond-length, binding energy, and Mulliken charge for armchair ZNONTs

Nanotube and stoichiometry	Tube diameter	Bond-length distribution (Å)	Binding energy (eV/each atom)	Mulliken charge
ZnO(3,3)	5.490	1.938	3.523	Zn : 0.699
	5.497[a]	1.919[a]	3.347[a]	O : −0.699
($Zn_{36}O_{36}H_{12}$)	5.490[b]	1.921[b]		Zn : 0.741[a]
				O : −0.741[a]
ZnO(4,4)	7.350	1.930	3.634	Zn : 0.705
				O : −0.704
($Zn_{48}O_{48}H_{16}$)	7.310[a]	1.914[a]	3.375[a]	Zn : 0.752[a]
				O : −0.752[a]
ZnO(5,5)	9.160	1.927	3.645	Zn : 0.709
	9.114[a]	1.909[a]		O : −0.707
($Zn_{60}O_{60}H_{20}$)	9.056[b]	1.907[b]	3.383[a]	Zn : 0.752[a]
				O : −0.752[a]

[a] Wang et al. (2007)

[b] Xu et al. (2007)

considered for our current DFT calculation. The second term expresses the effect of the interactive forces. In Eq. 2, V_i is the Voronoi volume of atom i and is constructed by the perpendicular planes bisecting the lines between this atom and all of its neighboring atoms. Clearly, it is time-consuming to compute the Voronoi volume of each atom in the simulation system. Accordingly, Srolovitz et al. (1981) proposed the following formulation to obtain a sphere the volume of which is equal to the original Voronoi volume:

$$V_i = \frac{4\pi}{3} a_i^3$$
$$a_i = \frac{\sum_j r_{ij}^{-1}}{2\sum_j r_{ij}^{-2}} \quad (2)$$

where a_i is the average radius of atom i and r_{ij} is the distance between atom i and its neighboring atom, j.

The normal strain in the axial direction of the ZNONT is given by

$$\varepsilon = \frac{\overline{l_{z(t)}} - l_{z(0)}}{l_{z(0)}} \quad (3)$$

where $\overline{l_{z(t)}}$ is the length of the ZNONT in the axial direction following elongation and $l_{z(0)}$ is the initial length. The stress–strain relationship of the ZNONT can then be obtained from Eqs. 1 and 3.

Results and discussion

Only the calculated results of (4,4) ZNONT are shown to investigate the effect of uniaxial tension on the armchair ZNONT electronic properties. Figure 2 shows the profiles of uniaxial stress and the HOMO–LUMO (highest occupied molecular orbital and lowest unoccupied molecular orbital) gap at different strains. The axial stress is calculated by the atomic stress equation as introduced in Eq. 1. The length of (4,4) ZNONT after the complete relaxation by DFT method is defined as the referenced length at strain 0, where the axial stress is close to zero. Because this study focuses on the electronic properties of an intact ZNONT at different strains without the bond breakage, the maximal strain shown in Fig. 2 is about 15% and the maximal stress is 60.17 GPa, at which all Zn–O bonds are still intact. For the stress–strain profile, it is apparent that the stress increases linearly with the increase of strain and for the profile of HOMO–LUMO gap; the gap linearly decreases from 2.29 to 1.84 eV with an increase in axial strain from 0 to 15% before some Zn–O bonds begin to break. Consequently, Fig. 2 clearly demonstrates that the mechanical deformation of a (4,4) ZNONT significantly influences its electronic properties, and the electronic properties vary linearly with the increase of strain.

The variations of bond lengths and bond angles at different strains are shown in Fig. 3b, c, and the

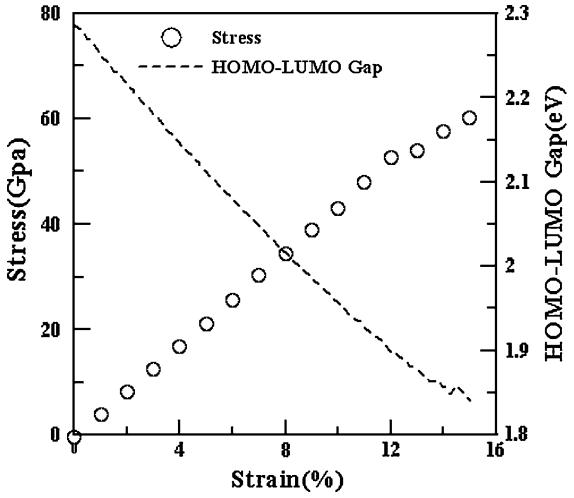

Fig. 2 *Hollow circle* shows uniaxial stress–strain curve for the (4,4) armchair ZNONT. *Dashed line* shows HOMO–LUMO gap variation with different strains

corresponding bond lengths and bond angles are depicted in Fig. 3a for the ZNONT at strain 0. The Zn–O bonds normal to the axial direction are designated as Bond **II** while those slanted to the axial direction are labeled as Bond **I**. The bond angles between Bond **II** (normal to the axial direction) and Bond **I** (slanted to the axial direction) are designated as Angle B, and the angle formed by two Bond **I** bonds are assigned as Angle A. The O atoms and their nearest three Zn atoms form pyramidal structures and are not in the same plane; the O atoms occupy the top vertices and point outwards, as reported in the previous study (Xu et al. 2007). In Fig. 3b, the value of radial buckling at different strains is also shown with the bond lengths at different strains. The definition of radial buckling β is shown as in Eq. 4:

$$\beta = r_O - r_{Zn} \tag{4}$$

where r_O and r_{Zn} are the mean radii of the O and Zn cylinders, respectively. If the value of radial buckling approaches zero, the Zn and O atoms will be located on the same cylindrical surface of ZNONT, while the positive value indicates that the ZNONT consists of two cylindrical surfaces, where the O atoms are situated on the outer surface. Regarding Fig. 3b, one can see that the lengths of Bond **I** and Bond **II** slightly increase from 1.93 to 1.97 Å with the increase of strain from 0 to 15%. As for the radial buckling, this parameter significantly decreases with

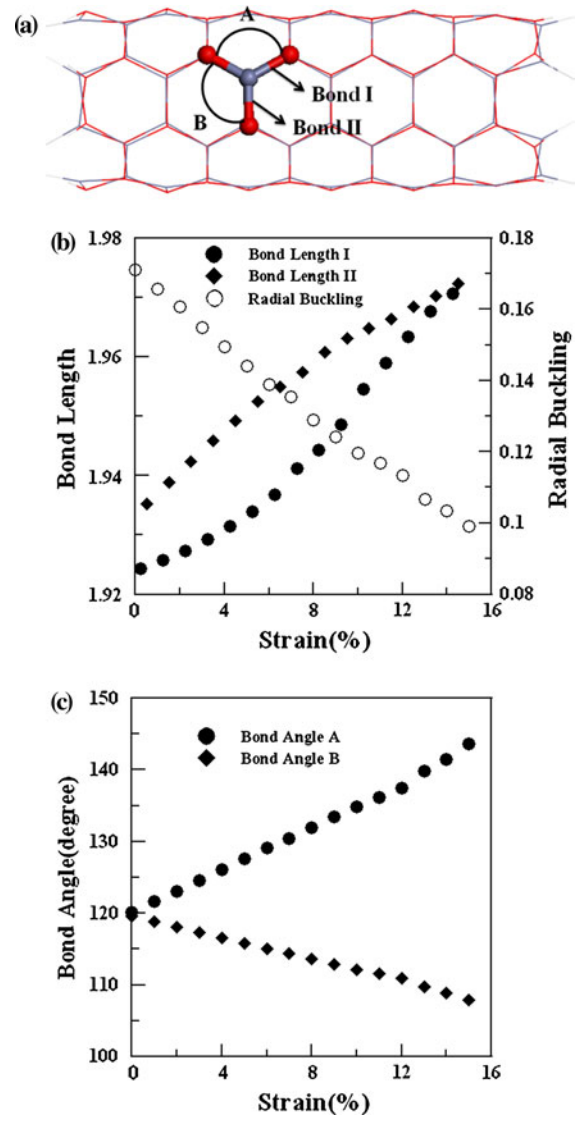

Fig. 3 **a** Bond angles and bond lengths. Bonds normal to axial are shown as Bond **II**; bonds slanted toward the axial are shown as Bond **I**. Bond angles are labeled as A, B, C, and D. *Red* atoms are oxygen, and *gray* atoms are zinc. **b** Variation of the radial buckling and bond lengths at different strains. **c** Variation of the bond angles shown at different strains. [Color figure can be viewed in the online issue]

the increase of strain, indicating that the Zn and O atoms are gradually forced to the same cylindrical surface when the ZNONT is under an increasing external stress. As shown in Fig. 3c for strain of 0–15%, Angle A dramatically increases from 120.14° to 143.59°, while Angle B significantly decreases from 119.58° to 107.87°. Since both Bond **I** and Bond **II** are only elongated about 2% at a strain of 15%,

the elongation of (4,4) ZNONT is mainly due to the altering of Angles A and B. In our previous study about the uniaxial tension of an armchair (4,4) silicon carbide nanotube (SiCNT) (Chen et al. 2010), at strain of 0–16% (where some Si–C bond breaking takes place), the Si–C bonds slanted to the tension direction remain constant while the Si–C bonds increase by 11% at strain of 16%. One characteristic angle formed by two slanted Si–C bonds increases from 120° to 137°, whereas the other characteristic angle decreases from 120° to 110°. Consequently, the elongation of the (4,4) SiCNT is mainly due to the variation of bond angles as well as the elongation of the slanted bonds. The Si–C bonds of the SiCNT originate from the orbital overlap of Si 3*p* and C 2*p*, leading to a covalent π bond. For ZNONT, the bond between Zn and O atoms mainly comes from the ionic bond, which has no directionality. To relax the nanotube structure under tension, an adjustment of angles, bond lengths, or both is required. For nanotubes with covalent bonds such as CNTs and SiCNTs, the directionality of the covalent bond causes significant variations in bond angles as well as a dramatic increase in bond length to make nanotube longer in the uniaxial direction during the tension process. The variation of bond angles will decrease the overlap of *p* orbitals and increase the binding energy. To get a more stable structure and avoid binding energy decreasing too much from only adjusting the bond angles, the elongation of covalent bonds slanted to the uniaxial direction will take place to make nanotube longer during the tension. This deformation mechanism can be also seen in the previous studies for CNTs (Song et al. 2009; Ebrahimi et al. 2008), where the bond length and bond angle undergo a significant change during the tension process. Even for graphene nanoribbons under uniaxial tension in the armchair or zigzag direction, the significant bond elongation as well as the variations of two characteristic bond angles are responsible for making the nanoribbon longer during the course of tension (Zhao et al. 2009). However, for nanotubes with ionic bonds such as the ZNONT of the current study, the directionality for the ionic bond has no significant effects on the bonding strength, but the distance between the anion and cation atoms has a critical influence on the binding energy. Consequently, the Zn–O bond lengths under different strains are very close to the equilibrium distance for the (4,4) ZNONT at strain of 0%, indicating the increase in the length of a (4,4) ZNONT under tension mainly originates from the variation of bond angles to make the nanotube longer. A previous study of structure transitions of a ZnO single crystal under tension also indicated that the Zn–O bond lengths remain almost constant during the structure transitions (Xu et al. 2009). One can also see the same deformation mechanism for a TiO_2 nanowire under the uniaxial tension by molecular dynamics simulation in Dai's study. Although necking behavior was observed and some Ti–O bonds broke during the tension, the average bond length also remained constant (Dai et al. 2009).

Figure 4 shows Mulliken charges of Zn 32 atom and O 30 atom at different strains. Zn 32 and O 30 atoms are a Zn atom and an O atom located in the middle part of the ZNONT, as shown in Fig. 1. At a strain of 0%, the charges of Zn 32 and O 30 were about 0.705 and −0.705 *e*, which are in agreement with those in a previous study (Wang et al. 2007). When the strain increased from 0 to 15%, both the Mulliken charges of Zn 32 and O 30 decrease by 0.007 e because the Zn–O bond length only slightly elongates by 2% during the course of tension. However, for covalently bonded nanotubes such as SiCNT (Chen et al. 2010), the Mulliken charges of Si and C atoms also turn out to be less ionic with the increase of axial strain from 0 to 16%. This larger electron variation is due to the significant increase in

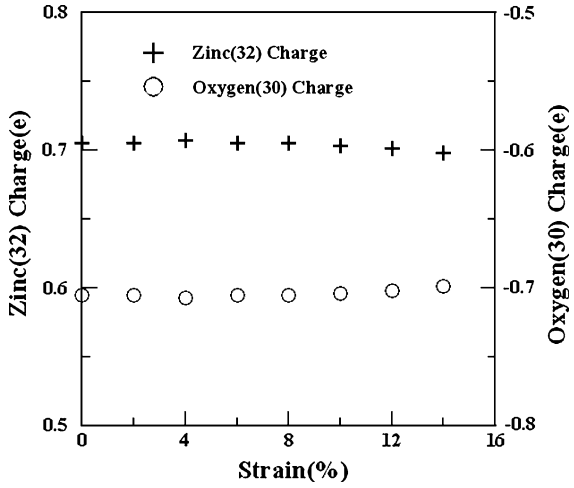

Fig. 4 Variation of the calculated atom charge of the single wall ZNONT. The *hollow circle* shows charge variation of O(30), and the *cross symbol* shows Zn(32)

the covalent bond length, which decreases the electron overlap between Si and C atoms during the tension process.

The profiles of partial density of states (PDOS) for Zn 32 and O 30 atoms were further studied to demonstrate the strain effect on the electronic structure of the ZNONT. Figure 5a–c shows the PDOS profiles of different orbitals of Zn 32 and O 30 atoms at strains of 0, 7.5, and 15%. It is apparent that the 2*s* orbital of O 30 atom nearly fails to hybridize with other orbitals and exhibits a prominent peak at about −17 eV at different strains. Between 0 and −4 eV, PDOS profiles indicate the orbital hybridization of O 2*p* and Zn 3*d* with a small amount of Zn 4*p* and Zn 4*s*. One can also see from PDOS profiles that O 2*p* orbital contributes more to the occupied states near the Fermi level and grabs electron from the Zn 3*d* orbital. Consequently, oxygen atoms have negative charges and zinc atoms possess positive charges, which can be seen in Fig. 4. At strains of 7.5 and 15%, the unoccupied states undergo slight left-shift toward the Fermi level, resulting in the small decrease in the HOMO–LUMO gap, as shown in Fig. 2.

The differential electron density (or so called "deformation density") at the iso-value of 0.04 and Mayer bond orders (BO) of three Zn–O bonds at three different strains are shown in Fig. 6a–c. The differential electron density is defined as the electron density distribution of ZNONT subtracting the electron density distributions of isolated O atoms and isolated Zn atoms. The isosurface around the O 30 atom indicates that the extra electron will transfer from Zn atoms to O atoms and accumulate around O atoms after a ZNONT forms from isolated O and Zn atoms. As can be seen from Fig. 6, the change of deformation density is not clear at different strains, which also reflects the fact that the changes of Zn and O charges are not significant, as shown in Fig. 4.

The value of the Mayer bond order between two atoms is very close to the corresponding classical bond number between these two atoms, and a detailed introduction of Mayer bond order can be found in Mayer's study (Mayer 1986). The BO values are calculated within the first nearest neighbor atoms around a referenced atom, with this value becoming very small when the distance between the reference atom and its nearest neighbor atom is beyond the stable bond length. At strain of 0%, the BO values of

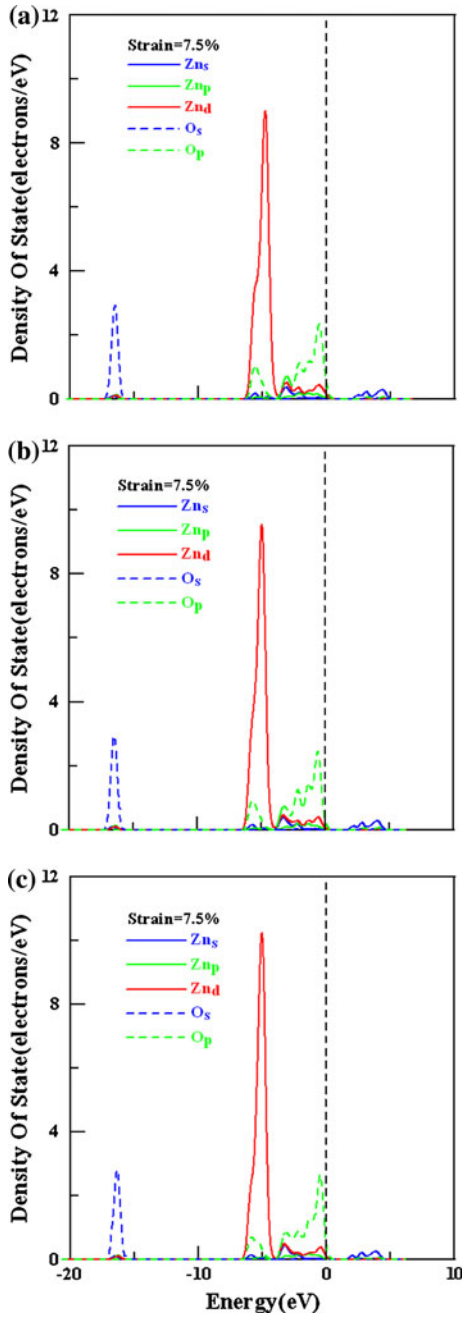

Fig. 5 PDOS profiles of Zn(32) and O(30) atoms. **a** strain = 0%, **b** strain = 7.5%, **c** strain = 15%

Bond **I** and Bond **II** are slightly different. The value of Bond **II** is slightly smaller than that of Bond **I** because the Bond **II** length is slightly longer than that of Bond I. At strain of 7.5%, the BO values of the two Bond **I** bonds remain constant in value while that of Bond **II** slightly decreases from 0.637 to 0.611.

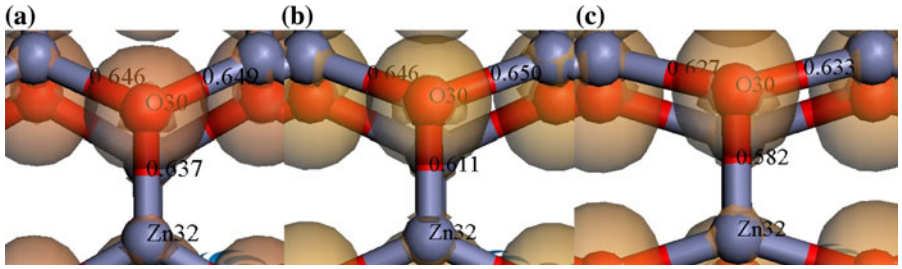

Fig. 6 Deformation density and Mayer bond orders shown at different strains: *a* strain = 0%, *b* strain = 7.5%, *c* strain = 15%

In Fig. 2, the elongation of Bond **I** is relatively longer than that of Bond **II**, so the smaller BO value at strain of 7.5% indicates the bonding strength of Bond **I** is slightly stronger than that of Bond **II**. At strain of 15%, the BO values of both Bonds **I** and **II** become smaller, indicating the three Zn–O bonds become weaker as strain is larger than 7.5%.

Conclusions

The DFT calculation has been performed to investigate the electronic properties of a (4,4) ZNONT under various magnitudes of tensile strain. The results have shown that the HOMO–LUMO gap of the (4,4) ZNONT displays a linear decrease with an increase of axial strain before some Zn–O bonds break. Regarding the radial buckling, the parameter significantly decreases with an increase in strain, indicating that the Zn and O atoms are gradually forced to the same cylindrical surface when the ZNONT is under an increasing external stress. Our results also indicate that the directionality for the ionic bond of (4,4) ZNONT is not so significant for the bonding strength, but the distance between the anion and cation atoms has a critical influence on the binding energy. Furthermore,the increase of the length of a ZNONT under tension mainly originates from the variations of bond angles to make the nanotube longer because the Zn–O bond lengths under different strains are very close to the equilibrium distance for the (4,4) ZNONT at strain of 0%. The result is different from the tension process of CNTs and SiCNTs in that both the bond lengths and bond angles undergo significant changes.

In addition, the PDOS of Zn 32 atom and O 30 atom of the ZNONT are explored at different strain levels. Our results demonstrate that the unoccupied states of both atoms are slightly left-shifted toward the Fermi level at strains of 7.5 and 15%, resulting in a slight decrease of the HOMO–LUMO gap. The change of Mulliken charge and deformation density also remains almost constant with the increasing strain. Finally, as the strain continuously increases from 0 to 15%, the BO analysis reveals that the value of Bond **I** and Bond **II** decreases from 0.649 to 0.627 and from 0.637 to 0.582, respectively. This result indicates that the bonding strength of Bond **I** and Bond **II** will be decreased.

Acknowledgment The authors would like to thank the (1) National Science Council of Taiwan, under Grant No. NSC98-2221-E-110-022-MY3 and NSC99-2911-I-110-512, (2) National Center for High-performance Computing, Taiwan, (3) National Center for Theoretical Sciences, Taiwan, for supporting this study.

References

An W, Wu XJ, Zeng XC (2008) Adsorption of O_2, H_2, CO, NH_3, and NO_2 on ZnO nanotube: a density functional theory study. J Phys Chem C 112:5747–5755

Chandra N, Namilae S, Shet C (2004) Local elastic properties of carbon nanotubes in the presence of Stone-Wales defects. Phys Rev B 69:094101

Chen HL, Ju SP, Lin JS, Zhao J, Chen HT, Chang JG, Weng MH, Lee SC, LeeW J (2010) Electronic properties of a silicon carbide nanotube under uniaxial tensile strain: a density function theory study. J Nanopart Res 12:2919–2928

Chou HC, Rohatgi A, Jokerst NM, Kamra S, Stock SR, Lowrie SL, Ahrenkiel RK, Levi DH (1996) Approach toward high efficiency CdTe/CdS heterojunction solar cells. Mater Chem Phys 43:178–182

Chu XF, Jiang DL, Djurisic AB, Yu HL (2005) Gas-sensing properties of thick film based on ZnO nano-tetrapods. Chem Phys Lett 401:426–429

Chubachi N (1976) ZnO films for surface acoustooptic devices on nonpiezoelectric substrates. Proc IEEE 64:772–774

Dai L, Sow CH, Lim CT, Cheong WCD, Tan VBC (2009) Numerical investigations into the tensile behavior of

TiO_2 nanowires: structural deformation, mechanical properties, and size effects. Nano Lett 9:576–582
Das R, Ray S (2003) Zinc oxide—a transparent conducting IR-reflector prepared by rf-magnetron sputtering. J Phys D-Appl Phys 36:152–155
Delley B (1990) An all electron numerical method for solving the local density functional for polyatomic molecules. J Chem Phys 92:508–517
Delley B (2000) From molecules to solids with the DMol(3) approach. J Chem Phys 113:7756–7764
Ebrahimi A, Ehteshami H, Mohammadi M (2008) Density functional calculations of response of single-walled armchair carbon nanotubes to axial tension. Comput Mater Sci 41:486–492
Erkoc S, Kokten H (2005) Structural and electronic properties of single-wall ZnO nanotubes. Physica E 28:162–170
Ferekides C, Britt J (1994) CdTe solar cells with efficiencies over 15-percent. Sol Energy Mater Sol Cells 35:255–262
Fulati A, Ali SMU, Riaz M, Amin G, Nur O, Willander M (2009) Miniaturized pH sensors based on zinc oxide nanotubes/nanorods. Sensors 9:8911–8923
Gao PX, Wang ZL (2005) Nanoarchitectures of semiconducting and piezoelectric zinc oxide. J Appl Phys 97:044304
He JH, Hsin CL, Liu J, Chen LJ, Wang ZL (2007) Piezoelectric gated diode of a single ZnO nanowire. Adv Mater 19: 781–784
Huang MH, Mao S, Feick H, Yan HQ, Wu YY, Kind H, Weber E, Russo R, Yang PD (2001) Room-temperature ultraviolet nanowire nanolasers. Science 292:1897–1899
Jing LQ, Wang BQ, Xin BF, Li SD, Shi KY, Cai WM, Fu HG (2004) Investigations on the surface modification of ZnO nanoparticle photocatalyst by depositing Pd. J Solid State Chem 177:4221–4227
Ju SP, Wang YC, Lien TW (2011) Tuning the electronic properties of boron nitride nanotube by mechanical uniaxial deformation: a DFT study. Nano Res Lett 6:160
Kaniber SM, Song L, Kotthaus P, Holleitner AW (2009) Photocurrent properties of freely suspended carbon nanotubes under uniaxial strain. Appl Phys Lett 94:261106
Keis K, Lindstrom H, Magnusson E, Hagfeldt A, Lindquist SE (2002) A 5% efficient photo electrochemical solar cell based on nanostructured ZnO electrodes. Sol Energy Mater Sol Cells 73:51–58
Kluth O, Rech B, Houben L, Wieder S, Schope G, Beneking C, Wagner H, Loffl A, Schock HW (1999) Texture etched ZnO: Al coated glass substrates for silicon based thin film solar cells. Sens Acutaors B 351:247–253
Kong XH, Sun XM, Li XL, Li YD (2003) Catalytic growth of ZnO nanotubes. Mater Chem Phys 82:997–1001
Kong T, Chen Y, Ye YP, Zhang K, Wang ZX, Wang XP (2009) An amperometric glucose biosensor based on the immobilization of glucose oxidase on the ZnO nanotubes. Sens Actuators B Chem 138:344–350
Langreth DC, Perdew JP (1980) Theory of nonuniform electronic systems. 1. Analysis of the gradient approximation and a generalization that works. Phys Rev B 21:5469–5493
Liao L, Lu HB, Li JC, He H, Wang DF, Fu DJ, Liu C, Zhang WF (2007) Zn-assisted synthesis and photoluminescence properties of MgO nanotubes. J Phys Chem C 111: 1900–1903
Liu P, She GW, Liao ZL, Wang Y, Wang ZZ, Shi WS, Zhang XH, Lee ST, Chen DM (2009) Observation of persistent photoconductance in single ZnO nanotube. Appl Phys Lett 94:063120
Mao Y, Zhong J, Chen Y (2008) First principles study of the band structure and dielectric function of (6,6) single-walled zinc oxide nanotube. Physica E 40:499–502
Mayer I (1986) Bond orders and valences from ab initio wavefunctions. Int J Quantum Chem 29:477–483
Niemegeers A, Burgelman M (1997) Effects of the Au/CdTe back contact on IV and CV characteristics of Au/CdTe/CdS/TCO solar cells. J Appl Phys 81:2881–2886
Ozgur U, Alivov YI, Liu C, Teke A, Reshchikov MA, Dogan S, Avrutin V, Cho SJ, Morkoc H (2005) A comprehensive review of ZnO materials and devices. J Appl Phys 98:041301
Perdew JP, Burke K, Ernzerhof M (1996) Generalized gradient approximation made simple. Phys Rev Lett 77:3865–3868
Qin Y, Wang XD, Wang ZL (2008) Microfibre-nanowire hybrid structure for energy scavenging. Nature 451: 809-U5
Rao BB (2000) Zinc oxide ceramic semi-conductor gas sensor for ethanol vapour. Mater Chem Phys 64:62–65
Rodriguez JA, Jirsak T, Dvorak J, Sambasivan S, Fischer D (2000) Reaction of NO_2 with Zn and ZnO: Photoemission, XANES, and density functional studies on the formation of NO_3. J Phys Chem B 104:319–328
Sberveglieri G, Groppelli S, Nelli P, Giunta G, Tintinelli A (1995) A novel method for the preparation of NH_3 sensors based on ZnO–In thin films. Thin Solid Films 25:588–590
Sebastian PJ, Ocampo M (1996) A photodetector based on ZnCdS nanoparticles in a CdS matrix formed by screen printing and sintering of CdS and $ZnCl_2$. Sol Energy Mater Sol Cells 44:1–10
Shiri D, Kong Y, Buin A, Anantram MP (2008) Strain induced change of bandgap and effective mass in silicon nanowires. Appl Phys Lett 93:073114
Song XH, Liu S, Yan H, Gan ZY (2009) First-principles study on effects of mechanical deformation on outer surface reactivity of carbon nanotubes. Physica E 41:626–630
Srolovitz D, Maeda K, Vitek V, Egami T (1981) Structural defects in amorphous solids statistical analysis of a computer model. Philos Mag A 4:847–866
Tien LC, Sadik PW, Norton DP, Voss LF, Pearton SJ, Wang HT, Kang BS, Ren F, Jun J, Lin J (2005) Hydrogen sensing at room temperature with Pt-coated ZnO thin films and nanorods. Appl Phys Lett 87:3
Touskova J, Kindl D, Tousek J (1997) Preparation and characterization of CdS/CdTe thin film solar cells. Thin Solid Films 293:272–276
Wang ZL, Song JH (2006) Piezoelectric nanogenerators based on zinc oxide nanowire arrays. Science 312:242–246
Wang RM, Xing YJ, Xu J, Yu DP (2003) Fabrication and microstructure analysis on zinc oxide nanotubes. New J Phys 5:115
Wang XD, Zhou J, Song JH, Liu J, Xu NS, Wang ZL (2006) Piezoelectric-field effect transistor and nano-force-sensor based on a single ZnO nanowire. Nano Lett 6:2768–2772
Wang B, Nagase S, Zhao J, Wang G (2007) The stability and electronic structure of single-walled ZnO nanotubes by density functional theory. Nanotechnology 18:34570

Xu JQ, Pan QY, Shun YA, Tian ZZ (2000) Grain size control and gas sensing properties of ZnO gas sensor. Sens Actuators B Chem 66:277–279

Xu H, Zhang RQ, Zhang XH, Rosa AL, Frauenheim T (2007) Structural and electronic properties of ZnO nanotubes from density functional calculations. Nanotechnology 18:485713

Xu LZ, Liu YL, Zhou HB, Liu LH, Zhang Y, Lu GH (2009) Ideal strengths, structure transitions and bonding properties of a ZnO single crystal under tension. J Phys Condens Matter 21:495402

Yuan PF, Ding ZJ, Ju X (2008) Theoretical study on structural and elastic properties of ZnO nanotubes. Chin Phys Lett 25:1030–1033

Zhao H, Min K, Aluru NR (2009) Size and chirality dependent elastic properties of graphene nanoribbons under uniaxial tension. Nano Lett 9:3012–3015

Zhou Z, Li Y, Liu L, Chen Y, Zhang SB, Chen Z (2008) Size- and surface-dependent stability, electronic properties, and potential as chemical sensors: computational studies on one-dimensional ZnO nanostructures. J Phys Chem C 112:13926–13931

Zhu ZG, Chutia A, Sahnoun R, Koyama M, Tsuboi H, Hatakeyama N, Endou A, Takaba H, Kubo M, Del Carpio CA, Miyamoto A (2008) Theoretical study on electronic and electrical properties of nanostructural ZnO. Jpn J Appl Phys 47:2999–3006